

UC Berkeley

UC Berkeley Previously Published Works

Title

Signatures of the Bromine Atom and Open-Shell Spin Coupling in the X-ray Spectrum of the Bromobenzene Cation

Permalink

<https://escholarship.org/uc/item/0qx3s9v0>

Journal

Journal of the American Chemical Society, 145(6)

ISSN

0002-7863

Authors

Epshtein, Michael

Tenorio, Bruno Nunes Cabral

Vidal, Marta L

et al.

Publication Date

2023-02-15

DOI

10.1021/jacs.2c12334

Copyright Information

This work is made available under the terms of a Creative Commons Attribution-NonCommercial License, available at <https://creativecommons.org/licenses/by-nc/4.0/>

Peer reviewed

Signatures of the Bromine Atom and Open-Shell Spin-Coupling in the X-ray Spectrum of Bromobenzene Cation

Michael Epshtein^{1,2}, Bruno Nunes Cabral Tenorio³, Marta L. Vidal³, Valeriu Scutelnic^{1,2}, Zheyue Yang¹, Tian Xue¹, Anna I. Krylov⁴, Sonia Coriani³, and Stephen R. Leone^{1,2,5*}

¹ Department of Chemistry, University of California, Berkeley, CA, 94720, USA

² Chemical Sciences Division, Lawrence Berkeley National Laboratory, Berkeley, CA, 94720, USA

³ DTU Chemistry - Department of Chemistry, Technical University of Denmark, DK-2800, Kongens Lyngby, Denmark

⁴ Department of Chemistry, University of Southern California, Los Angeles, California 90089, USA

⁵ Department of Physics, University of California, Berkeley, CA, 94720, USA

ABSTRACT: Table-top x-ray spectroscopy measurements at the carbon *K*-edge complemented by *ab initio* calculations are used to investigate the influence of the bromine atom on the carbon core-valence transitions in bromobenzene cation (BrBz⁺). The electronic ground state of the cation is prepared by resonance-enhanced two-photon ionization of neutral bromobenzene (BrBz) and probed by x-rays produced by high-harmonic generation (HHG). Replacing one of the hydrogen atoms in benzene with a bromine atom shifts the transition from the 1s_{C*} orbital of the carbon atom (C*) bonded to bromine by ~1 eV to higher energy in the x-ray spectrum compared to the other carbon atoms (C). The x-ray absorption spectra of neutral BrBz reveals the influence of the bromine atom on the x-ray absorption spectrum due to the 1s_{C*} orbital, while the influence of the bromine atom on the cation spectrum is even more prominent. The x-ray spectrum of the cation is dominated by two relatively intense transitions, the 1s_C → π* and the 1s_{C*} → σ*(C*-Br), where the second transition is enhanced relative to the neutral BrBz. In addition, a doublet peak shape for these two transitions is observed in the experiment. The 1s_C → π* doublet peak shape arises due to the spin coupling of the unpaired electron in the partially vacant π orbital (from ionization) with the two other unpaired electrons resulting from the transition from the 1s_C core orbital to the fully vacant π* orbitals. The 1s_{C*} → σ* doublet peak shape results from several transitions involving σ* and vibrational C*-Br mode activation following the UV ionization, which demonstrates the impact of the C*-Br bond length on the core-valence transition as well as the relaxation geometry of BrBz⁺.

INTRODUCTION

X-ray spectroscopy at the carbon *K*-edge is highly sensitive to the changes in molecular structure and orbital occupancy, delivering accurate information about the energy of core and valence orbitals of molecules containing carbon atoms. The ability to laser-produce tabletop HHG sources reaching up to 300 eV opened opportunities to implement the laser pump-probe technique with ultraviolet (UV) excitation probed by soft x-ray radiation in the carbon *K*-edge region with tens of femtosecond time resolution.^{1,2,3,4,5,6,7,8}

Recently, we applied this technique to measure the x-ray spectrum of the benzene radical cation (Bz⁺).⁹ Together with high-level calculations using equation-of-motion coupled-cluster singles and doubles theory (EOM-CCSD), this study provided insight into the electronic structure of benzene (Bz) and its cation.¹⁰ Comparison of the x-ray absorption spectra of neutral Bz and of Bz⁺ revealed a splitting of the two degenerate π* orbitals as well as an appearance of a new peak due to a new transition to the partially occupied π orbital resulting from the ionization. According to the calculations, the observed splitting in the cation spectrum was ascribed primarily to the spin coupling of the unpaired electron in the partially vacant π orbital with the unpaired electrons resulting from the excitation of one of the carbon 1s electrons to the vacant π* orbitals.^{9,10} Jahn-Teller relaxation causing symmetry distortion was also considered.

Replacing one of the hydrogen atoms of Bz by a bromine atom lowers the D_{6h} point-group symmetry of neutral Bz to C_{2v}, and also

lifts the near-degeneracies between the six core orbitals of the carbon atoms. In particular, the Br atom increases the transition energy of the carbon atom bonded to the bromine atom, here labeled as C*. The two highest occupied molecular orbitals, π(6b₂) and π(2a₂), result from a splitting of the highest degenerate π orbitals of Bz. The highest occupied molecular orbital (HOMO) π(6b₂), with the lowest binding energy of 8.992 eV,¹¹ shows partial bromine character.^{12,13,14} The major electron density of the π(6b₂) orbital is distributed among several atoms, the C* atom (0.46), the C atom that is in the para position to C* (0.5), the Br atom (0.47) and among the other C atoms (0.56).¹² The next lower π(2a₂), orbital of BrBz is noticeably shifted to lower energy (i.e., to higher binding energy, 9.663 eV) compared to the parent π orbital of Bz. The next two lower molecular orbitals are 11b₁ (σ_{Br}-type) and 5b₂ (π_{Br}-type) that are related to the 4p bromine lone pair orbitals, which are split due to the interaction with the benzene ring.^{12,13,14} The ionization energies from these two orbitals are 10.633 eV and 11.188 eV, respectively.¹³

The bromine atom affects the core level transition energies as well. Previous studies have shown that¹⁵ the 1s orbital of the carbon atom (C*) nearest to the bromine atom is shifted to higher binding energy by about 1.1 eV relative to the 1s orbitals of the other carbons (C), as shown in the orbital diagram of BrBz in Figure 1. The splitting of the other 1s_C orbitals due to lower symmetry of the benzene ring is much smaller.¹⁵ The different electron distribution in the valence and core levels due to bromine attachment leads to several changes in the x-ray spectrum of neutral BrBz compared to

Bz.¹⁵ The major change appears as a new peak related to the $1s_{C^*} \rightarrow \pi^*$ transition shifted to higher energy by about 1.1 eV from the most intense peak that corresponds to the $1s_C \rightarrow \pi^*$ transition, which is similar to the $1s_C \rightarrow \pi^*$ transition in the x-ray spectrum of neutral Bz.

The effect of substitution of the bromine atom (as well as other halogen atoms) in neutral aromatic rings on the core-valence transitions in the carbon *K*-edge region has been investigated in the past.^{15,16,17,18} In contrast, the influence of halogen atoms on the core-valence transitions at the carbon *K*-edge in the cations has not been studied before. In this work, we examine the influence of a bromine atom on the core-valence transitions in BrBz⁺ by comparing the experimental near-edge x-ray absorption fine structure spectrum (NEXAFS) of BrBz⁺ with the spectrum of neutral BrBz and with our recent spectrum of Bz⁺ in the same energy region,^{9,10} combined with electronic structure calculations. Specifically, we used the density functional theory/restricted open shell configuration interaction singles (DFT/ROCIS) method¹⁹ associated with molecular dynamics (MD) simulations adopting the B3LYP functional,²⁰ and the def2-TZVP basis set.²¹

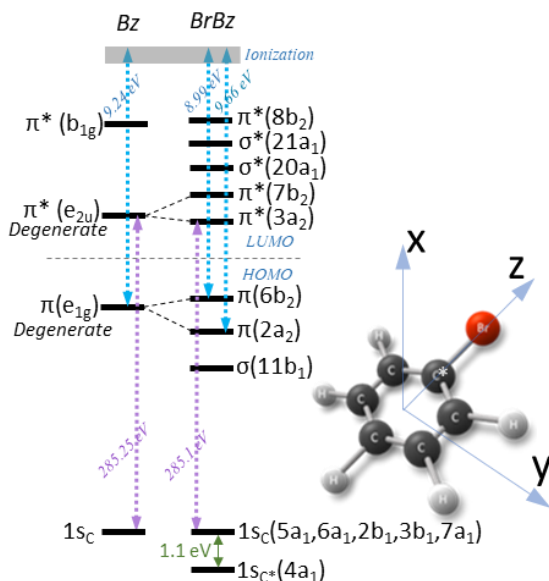


Figure 1. Schematic orbital diagram of neutral Bz and BrBz based on ref^{11,15} with relevant ionization energies and core-valence transition energies (the energy is not to scale). The geometry of BrBz and the coordinate system are shown on the right. The molecule is in the YZ plane with Br on the Z axis. The carbon atom binding to Br is labeled as C*.

RESULTS

The experimental spectrum of neutral BrBz, presented in Figure 2(a), is obtained from $A = \log(I_{\text{without Bz}} / I_{\text{with Bz}})$, where $I_{\text{without Bz}}$ and $I_{\text{with Bz}}$ are the transmitted signal of the broadband x-ray flux without BrBz molecules in the interaction region and with flow of BrBz molecules at room temperature, respectively, as described in detail previously.^{3,9} The spectrum matches well with previously reported results,¹⁵ and it agrees with our calculations, shown in red in Figure 2(b). The spectrum exhibits one dominant peak at 285.1 eV, labeled as A in Figure 2(a), followed by at least 4 discernable peaks of lower intensity, labelled B-E.

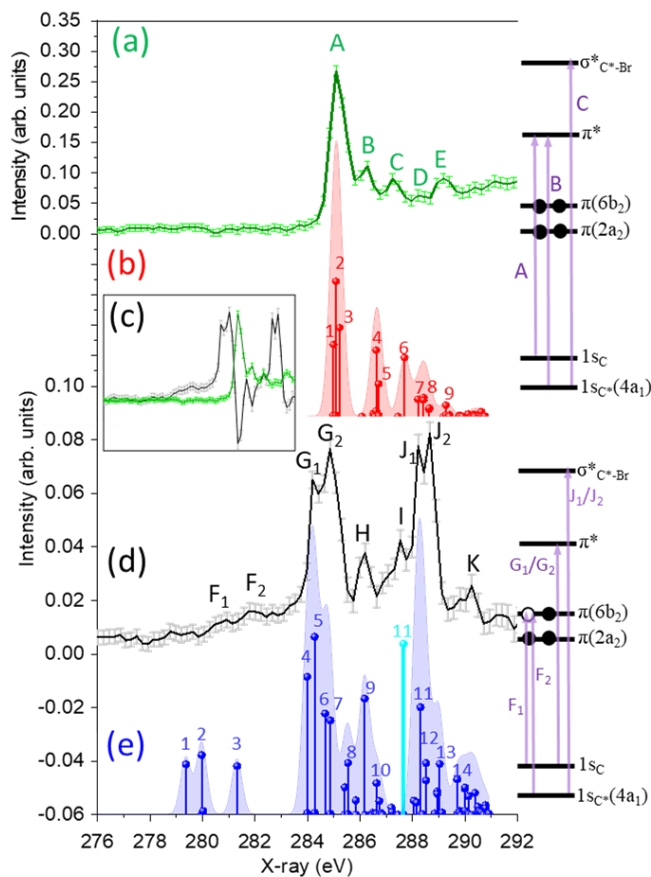


Figure 2. (a) Experimental NEXAFS spectrum of ground-state neutral BrBz (green line with light green error bars corresponding to 95% confidence interval limits). The spectrum is an average of 256 CCD images (1000 laser pulses per image). The full range of the same data is presented in the Supplementary Information (SI). (b) Calculated DFT-ROCIS transitions of neutral BrBz shown by red sticks and corresponding broadened spectrum (shifted by +10.2 eV and 0.45 eV Gaussian width for each transition). (c) Experimental NEXAFS spectra of neutral BrBz (green) and of BrBz⁺ (black). The spectrum is an average of 768 CCD images (see SI for details). (d) NEXAFS spectrum of BrBz⁺ obtained by adding 20% of the static neutral BrBz spectra (see SI for details) to the difference spectrum ΔA in (c), taken at ~ 1 ps delay, represented by the black line with grey error bars, and with the energy diagram on the right side. (e) Calculated DFT-ROCIS transitions of BrBz⁺ at relaxed geometry (blue sticks) and corresponding broadened spectrum (shifted by 9.2 eV and 0.45 eV Gaussian width for each transition). The calculations were performed with B3LYP/def2-TZVP without making use of symmetry point group. The cyan stick in (e) corresponds to the $1s_{C^*} \rightarrow \sigma^*(C^*-Br)$ transition at the Franck-Condon (FC) geometry. The full spectrum at FC geometry is shown in Figure S2 in SI. The energy diagram on the side illustrates the major transitions observed in the spectra.

Table 1. Transitions of neutral BrBz observed in the experimental spectrum in Figure 2(a) compared with the computed transitions shown as sticks in Figure 2(b). Calculated energies shifted by 10.2 eV to fit to the experimental spectrum.

Experiment		ROCIS-DFT		
Peak	Energy (eV)	Stick	Energy (eV)	Assignment
A	285.1	1	285.03	$1s_C(3b_1) \rightarrow \pi^*(3a_2)$ $1s_C(6a_1) \rightarrow \pi^*(7b_2)$
		2	285.22	$1s_C(2b_1) \rightarrow \pi^*(3a_2)$ $1s_C(5a_1) \rightarrow \pi^*(7b_2)$
		3	285.24	$1s_C(7a_1) \rightarrow \pi^*(7b_2)$
B	286.2	4	286.56	$1s_C^*(4a_1) \rightarrow \pi^*(7b_2)$
		5	286.64	$1s_C(3b_1) \rightarrow \sigma^*(20a_1)$
C	287.1	6	287.57	$1s_C(4a_1) \rightarrow \sigma^*(20a_1)$
D	288.0	7	288.05	$1s_C(7a_1) \rightarrow \sigma^*(21a_1)$
		8	288.24	$1s_C(3b_1) \rightarrow \sigma^*(20a_1)$ $1s_C(3b_1) \rightarrow \sigma^*(21a_1)$
E	288.5	9	289.04	$1s_C(2b_1) \rightarrow \sigma^*(21a_1)$

In accordance with the previous work, we assign peak A as due to transitions from the $1s_C$ orbitals (i.e., the $1s$ orbitals of the C atoms not bound to Br atom) to the two lowest unoccupied π^* molecular orbitals,¹⁵ similar to the $1s_C \rightarrow \pi^*$ transition observed at 285.25 eV in the x-ray spectrum of Bz.^{9,10,13,15} (See Table 1 for details on the peak assignments and calculated energies).

We ascribe the next, less intense, observed transition—peak B at 286.2 eV—to an electronic transition from the $1s_{C^*}$ orbital ($4a_1$) to π^* . Hitchcock *et al.* also assigned this peak to a $1s_{C^*} \rightarrow \pi^*$ transition and concluded that the energy shift between peak A and B occurs primarily due to the chemical shift (of about 1.1 eV stronger binding) of the $1s_{C^*}$ orbital relative to the $1s_C$ orbitals, while the energy of the π^* orbital is insensitive to bromine substitution. Similar behavior was observed in chlorobenzene (ClBz),²² iodobenzene (IBz), and fluorobenzene (FBz).¹⁵

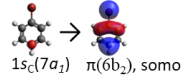
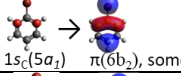
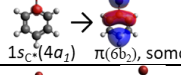
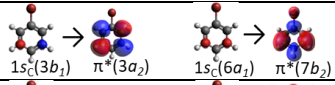
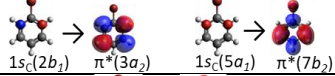
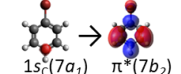
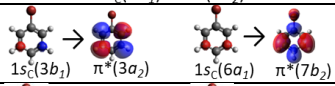
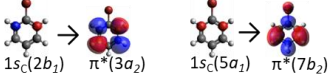
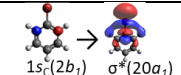
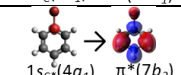
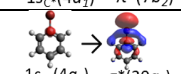
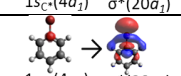
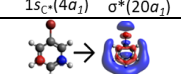
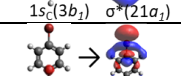
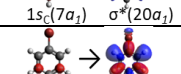
The influence of the halogen substitution on the $1s$ orbital of the nearest carbon atom (C^*) has been explored in several other studies.^{16,17,18} For instance, by replacing the number of F atoms with hydrogens, Hitchcock *et al.*¹⁶ and Plashkevych *et al.*¹⁸ showed that the relative intensities of $1s_C \rightarrow \pi^*$ and $1s_{C^*} \rightarrow \pi^*$ transitions are affected by the relative number of C and C^* carbon sites. Interestingly, the position of the $1s_C \rightarrow \pi^*$ and $1s_{C^*} \rightarrow \pi^*$ transitions was almost not affected by the change in the number of F atoms,

indicating the localized behavior of the $1s_C$ and $1s_{C^*}$ orbitals and that the energy of the π^* orbital is unaffected by the substitution. In addition, it was proposed that a $1s_C \rightarrow 3s$ transition contributes to the intensity of the peak assigned to the $1s_{C^*} \rightarrow \pi^*$ transition.^{16,17} Similarly, $1s_C \rightarrow \pi^*$ and $1s_{C^*} \rightarrow \pi^*$ transitions are reported in the x-ray spectrum of C_3H_2Br to have similar amplitude ratio, emphasizing the dependence of the peak intensities on the number of core sites and the localized behavior near the C^*-Br bond.²³ Our computed $1s_{C^*} \rightarrow \pi^*$ transition energy matches well the experimental result, aside from a slightly larger separation between peak A and B, as can be seen from Figure 2(a) and (b). Next, peak C in Figure 2(a), observed to be at around 287 eV. The calculation suggest that this peak related to $1s_{C^*} \rightarrow \sigma^*(C^*-Br)$ transition labeled as 6 in Figure 2(b), with a good agreement to previous results.²⁴ The other transitions have previously been described as $1s_C \rightarrow 5p$ (288.0 eV), $1s_C \rightarrow 4d$ and $1s_C \rightarrow 6s$ (289.0 eV), corresponding to peaks D, and E as shown in Table 1, and to sticks 7, 8 from our calculation. The binding energy reported from previous works to be 290.5 and 291.3 eV from $1s_C$ and $1s_{C^*}$, respectively.^{15,25}

The black line in Figure 2(d) shows the absorption spectrum of $BrBz^+$. The spectrum is obtained from $\Delta A = \log(I_{\text{without UV}} / I_{\text{with UV}})$, where $I_{\text{without UV}}$ and $I_{\text{with UV}}$ are the transmitted signal of the x-ray flux without UV and with UV, respectively, after adding back 20% of neutral spectrum. The UV pulses at 267 nm ionize the molecule by resonance enhanced two-photon ionization (1+1 REMPI) after being focused with a 45 cm f.l. lens where the UV pulse energy is $\sim 25 \mu J$. The broadband HHG pulse near the carbon K-edge probes the prepared $BrBz^+$ after ~ 1 ps time delay. Two-photon 267 nm excitation is in resonance with the first ionized state ($E_{\text{Ion}}=8.992$ eV),²⁶ in which one electron is removed from the π orbital, creating a hole in the highest $\pi(6b_2)$ orbital. Consequently, the lowest-energy transition (at ~ 281 eV) in the cation from a core orbital is of $1s_C \rightarrow \pi$ character, while a second transition (of $1s_{C^*} \rightarrow \pi$ character) is expected to be ~ 1 eV higher in energy. Evidence of these two transitions is just discernible in the experimental spectrum. The core-to-SOMO (singly occupied MO) $1s_C \rightarrow \pi$ transition in Bz^+ was found to be relatively weak in our previous study,⁹ and it is expected to be even weaker in $BrBz^+$ because the intensity is redistributed between two transitions from $1s_C$ and $1s_{C^*}$ orbitals, in addition to possibly a more diffuse vibrational structure due to higher available energy (E_{av}) after ionization ($E_{\text{ph}} - E_{\text{Ion}} = E_{\text{av}} = 0.25$ eV compared to 0.07 eV in Bz^+). Indeed, theory shows the presence of two major transitions from $1s_C$, namely $1s_C(7a_1) \rightarrow \pi(6b_2)$, $1s_C(5a_1) \rightarrow \pi(6b_2)$, in addition to the $1s_{C^*}(4a_1) \rightarrow \pi(6b_2)$ transition at higher energy (blue sticks labelled 1, 2 and 3 in Figure 2(e) and in Table 2).

The next two peaks of nearly equal intensity, toward higher energy, a doublet peak structure, are labeled as G_1 and G_2 , at 283.9 and 284.55 eV (0.65 eV difference) and are readily seen in the raw data inset in Figure 2(c) for $BrBz^+$ even before adding back 20% of the neutral benzene spectrum. These peaks are red-shifted compared to peak A ($1s_C \rightarrow \pi^*$) of $BrBz$, and it is therefore reasonable to assign them to $1s_C \rightarrow \pi^*$ transitions, similar to the previously reported Bz^+ spectrum.⁹ Indeed, the transitions from $1s_C$ to the lowest π^* orbital observed in the x-ray spectrum of neutral Bz and of $BrBz$ are remarkably similar and the

Table 2. Transitions of BrBz⁺ observed in the experimental spectrum in Figure 2(d) and in the calculated sticks in Figures 2(e), the calculated transition at the FC geometry (highlighted by yellow) not observed in the experimental spectrum due to a long-time delay. The highlighted Sticks 4,7 (orange) and 5,8 (blue) are different in energy due to spin coupling. Calculated energies shifted by 9.2 eV to fit to the experimental spectrum.

Experiment		ROCIS-DFT		
Peak	Energy (eV)	Stick	Energy (eV)	Assignment
F	280.70 281.80	1	279.37	 $1s_c(7a_1) \rightarrow \pi(6b_2), \text{somo}$
		2	279.97	 $1s_c(5a_1) \rightarrow \pi(6b_2), \text{somo}$
		3	281.32	 $1s_c(4a_1) \rightarrow \pi(6b_2), \text{somo}$
G ₁	284.20	4	283.99	 $1s_c(3b_1) \rightarrow \pi^*(3a_2)$ $1s_c(6a_1) \rightarrow \pi^*(7b_2)$
		5	284.27	 $1s_c(2b_1) \rightarrow \pi^*(3a_2)$ $1s_c(5a_1) \rightarrow \pi^*(7b_2)$
G ₂	284.85	6	284.68	 $1s_c(7a_1) \rightarrow \pi^*(7b_2)$
		7	284.87	 $1s_c(3b_1) \rightarrow \pi^*(3a_2)$ $1s_c(6a_1) \rightarrow \pi^*(7b_2)$
		8	285.49	 $1s_c(2b_1) \rightarrow \pi^*(3a_2)$ $1s_c(5a_1) \rightarrow \pi^*(7b_2)$
H	286.20	9	286.18	 $1s_c(2b_1) \rightarrow \sigma^*(20a_1)$
		10	286.63	 $1s_c(4a_1) \rightarrow \pi^*(7b_2)$
FC		11'	287.66	 $1s_c(4a_1) \rightarrow \sigma^*(20a_1)$
J ₁	288.20	11	288.31	 $1s_c(4a_1) \rightarrow \sigma^*(20a_1)$
J ₂	288.60	12	288.52	 $1s_c(3b_1) \rightarrow \sigma^*(21a_1)$
		13	289.04	 $1s_c(7a_1) \rightarrow \sigma^*(20a_1)$
k	290.2	14	289.70	 $1s_c(6a_1) \rightarrow \pi^*(8b_2)$

energy of the π^* orbital is not affected by replacing halogen atoms as pointed out above; the same is expected to occur in the x-ray spectrum of the cations.

The doublet peak structure of G₁ and G₂ can be (partly) explained by the spin coupling of the three unpaired electrons,^{27,28} as recently observed in N₂⁺,²⁹ CO⁺,³⁰ and in Bz⁺.^{9,10} The splitting of the main peak in Bz⁺ is more than 1 eV, caused mostly by spin coupling between unpaired electrons in 1s_c, π and π^* orbitals as

substantiated by the calculations.¹⁰ The theoretical results have shown that Jahn-Teller (JT) shifts for Bz⁺ cause a much smaller splitting of the two degenerate π^* orbitals. Here, we attribute the observed doublet peak structure of BrBz⁺ to a similar spin coupling effect. The calculations revealed the presence of two transitions from two different 1s_c orbitals to π^* (sticks 4 and 5 in Figure 2(e) and corresponding assignments in Table 2), followed by a transition 1s_c(7a₁)→ π^* (3a₂) (stick 6) plus two transitions, labeled as sticks 7 and 8, involving the same orbitals as sticks 4,5 but with different spin of the unpaired electron in the π orbital (SOMO).

The next peak, labeled as H, fits well to the calculated 1s_c→ σ^* (C*-Br) transition (labelled as stick 9), with an additional contribution from a 1s_c→ π^* transition (stick 10). This behavior is quite similar to the neutral BrBz, while in BrBz⁺ the calculations show a more dominant influence of the transition to the σ^* (C*-Br) orbital. The next dominant transitions in the experimental spectrum are labeled as peaks J₁ and J₂, at 288.2 and 288.60 eV. In the previously reported x-ray spectrum of Bz⁺,⁹ we did not observe major peaks in this energy region and, therefore, we consider these transitions as strongly related to the bromine atom.

The effect of the bromine atom on the transitions related to the benzene ring is small, as can be seen by comparing the 1s_c→ π^* transition in the neutral Bz and BrBz x-ray spectra, which are similar. The same conclusion can be drawn from fluorinated benzene x-ray spectrum as mentioned previously,¹⁶ as a change in the number of the fluorine atoms had no effect on the energy of the 1s_c→ π^* transition. Therefore, the major effect of the bromine atom should be related to the C*-Br bond, in particular, on the transition to the orbitals related to this bond, for example 1s_c→ σ^* (C*-Br).

Above 287 eV, the experimental spectrum of the cation is dominated by the split-band J₁, J₂. According to our calculations, the most intense transition in this region is due to 1s_c→ σ^* (C*-Br), which in neutral BrBz corresponds to band C. We note that after ionization a major change of the cation's ground-state structure relative to the neutral ground state BrBz appears to be the C*-Br bond length, which changes from 1.9189 Å to 1.8439 Å (according to our calculated geometries obtained at the EOM-CCSD/aug-cc-pVTZ level, see in our supplementary file). This could be one of the reasons for the dramatic change in transition intensities for peaks J₁, J₂ compared to peak C and D in neutral BrBz.

Moreover, the transition to a σ^* (C*-Br) orbital may be affected by vibrational motion of the C*-Br bond. Two-photon excitation imparts vibrational excitation to the cation, even though the exact determination of the excited vibrational state is difficult due to the low spectral resolution of the experimental system, the spectral width of the UV pulses, and due to the high density of the vibrational states at 9.24 eV. However, since the two-photon ionization process is sensitive to the vibrational mode(s) of the (intermediate) electronic excited state of neutral BrBz reached by the first photon excitation, ¹A₁ → ¹B₂ ($\pi\pi^*$), where the density of possible vibrational states is lower (in the region reached by one photon), it is possible to predict which vibrational modes of the cation are activated. The transition from the electronic ground state to the ground vibrational state of ¹B₂ is 4.586 eV. With the first photon (4.64 ± 0.08 eV) it is thus possible to reach the vibrational ground state and excite the C₆H₅-Br stretching mode (ν_{6a} = 0.03645 eV) of the electronic intermediate state (¹B₂). It is likely that excited vibrational states of the cation involve the C₆H₅-Br stretching mode (ν_{6a} at 0.047 eV for BrBz⁺ in the electronic ground state) alone or in combination with other modes, as shown in One-Photon Mass-Analyzed Threshold Ionization (MATI) spectra.³¹ The excited C*-Br stretching mode may influence the x-ray spectrum by shifting 1s_c→ σ^* (C*-Br) transition energies and their

intensities, as we observe in BrBz⁺ compared to the neutral BrBz. DFT-ROCIS calculations based on molecular dynamics simulations have been used to demonstrate the high sensitivity of the 1s_C*→σ*(C*-Br) transition to the stretching mode of the C*-Br bond. The results of these calculations, shown in Figure S.6, also illustrate a high sensitivity of the position of the 1s_C*→σ*(C*-Br) transition to the C*-Br bond length. This is also seen by comparing the calculated x-ray spectrum of BrBz⁺ at FC geometry with the spectrum at the relaxed geometry of the cation, in particular, the difference in the position of the cyan stick 11' in Figure 2(e), obtained at FC geometry, and stick 11 (peak J₁), which is the same transition but at the relaxed geometry. The enhanced sensitivity in energy is observed mostly for the 1s_C*→σ*(C*-Br) transition, while most of the other transitions remain at same energy, as Figure S.6 shows. Based on these results, one can tentatively rationalize the observed double-peaked structure of band J by the initial vibrational C*-Br stretching mode, since the molecule spends most of the time at two different bond lengths along the stretching mode of C*-Br bond, in addition to the contribution of the other transitions labeled as sticks 12 and 13. The precise assignment of other peaks, including peak I and K, is difficult due to low intensities and many different possibilities involving different core orbitals and spin coupling effects.

Preparation of BrBz⁺ in the electronic ground state and exclusion of possible contributions due to both one-photon excitation of neutral BrBz and photodissociation processes, as well as three-photon electronically-excited cations, are expected to be small enough compared to the discussed observations of this work, similar to our previous study with benzene.⁹ The cross section for the intermediate electronic resonance state [¹A₁→¹B₂(ππ*), 4.586 eV]³¹ of BrBz with one photon (266.8 nm) is 3 × 10⁻¹⁹ (cm²/molecule),¹¹ slightly greater than in Bz, (10⁻²⁰-10⁻²¹ cm²/molecule),^{32,33} but the major process, driven by fs pulses around 266 nm, is REMPI (1+1).³⁴ Preparation of excited electronic states of BrBz⁺ may be possible only by transferring an electron from a lower orbital and requiring 3 photons, as shown in the schematic orbital diagram of neutral BrBz in Figure 2. Moreover, excitation from the lower orbital with a 267 nm photon is below the first resonance (excitation to first electronic state) and therefore expected to be a significantly less probable process. From this we conclude that the major probed molecules by the x-ray flux are bromobenzene cations in the ground electronic state.

CONCLUSION

This work investigated the carbon *K*-edge spectrum of BrBz⁺, recorded following resonance ionization with two UV photons on neutral BrBz. The influence of the bromine atom on the x-ray spectrum of the BrBz⁺ is examined together with the spin coupling of the partially vacant 1s core orbital, the partially occupied π orbital, and the partially occupied π* orbital. In particular, the partially occupied π orbital leads to relatively weak 1s_C→π and 1s_C*→π transitions, while the 1s_C→π* transitions are observed as a first dominant peak slightly shifted to lower energy compared to corresponding transitions in the neutral BrBz, similarly to the Bz⁺ x-ray spectrum. Our results are supported by theoretical calculations by the ROCIS-DFT method. An additional relatively intense doublet peak is observed at higher energy and is assigned to the 1s_C*→σ*(C*-Br) transition of the cation. This transition demonstrates the significant influence of the bromine atom on the x-ray spectrum of BrBz⁺ compared to Bz⁺ and to neutral BrBz. The calculated spectrum reproduces the experimental features, but the big challenge of accurate calculations in large molecules remains together with a need for a better understanding of the spin coupling effect.

The new peaks, J₁/J₂ clearly demonstrate the influence of the bromine atom on the 1s_C*→σ*(C*-Br) transition in BrBz⁺ and maybe some contribution from 1s_C*→σ*(C-Br) transition. Thus, the ionization from the π(6b₂) orbital, which has bromine character has an impact on the C*-Br bond length and charge distribution near C*-Br bond, leading to a higher transition probability for 1s_C*→σ*(C*-Br). Moreover, the experimental and calculated spectra show a strong influence on the core to valence transition energy of the C*-Br bond length that is altered from the relaxed geometry of the BrBz⁺ and from the C*-Br vibrational stretching mode, which is highly active in BrBz⁺. On the other hand, the influence of the bromine atom on the rest of the benzene ring, and in particular on the transition to the π* orbital, is small.

AUTHOR INFORMATION

Corresponding Author

*srl@berkeley.edu

ACKNOWLEDGMENT

M.E., V.S., Z.Y., T.X., and S.R.L. gratefully acknowledge the generous support from the U.S. Department of Energy, Office of Science, Office of Basic Energy Sciences (Contract No. DEAC02-05CH11231), the gas phase chemical physics program through the Chemical Sciences Division of Lawrence Berkeley National Laboratory.

V.S. acknowledges support from the Swiss National Science Foundation (P2ELP2_184414).

B.N.C.T. acknowledges support from the European Union's Horizon 2020 Research and Innovation Programme under the Marie Skłodowska-Curie Individual Fellowship (Grant Agreement No. 101027796).

A.I.K. acknowledges financial support by the U.S. National Science Foundation through the CHE-2154482 grant.

M.L.V. and S.C. acknowledge financial support from the Independent Research Fund Denmark-Natural Sciences, DFF-RP2 grant no. 7014-00258B.

REFERENCES

- (1) Bhattacharjee, A.; Leone, S. R. Ultrafast X-Ray Transient Absorption Spectroscopy of Gas-Phase Photochemical Reactions: A New Universal Probe of Photoinduced Molecular Dynamics. *Acc. Chem. Res.* **2018**, *51* (12), 3203–3211.
- (2) Pertot, Y.; Schmidt, C.; Matthews, M.; Chauvet, A.; Huppert, M.; Svoboda, V.; Von Conta, A.; Tehlar, A.; Baykusheva, D.; Wolf, J.-P. Time-Resolved X-Ray Absorption Spectroscopy with a Water Window High-Harmonic Source. *Science* **2017**, *355* (6322), 264–267.
- (3) Attar, A. R.; Bhattacharjee, A.; Pemmaraju, C. D.; Schnorr, K.; Closser, K. D.; Prendergast, D.; Leone, S. R. Femtosecond X-Ray Spectroscopy of an Electrocyclic Ring-Opening Reaction. *Science* **2017**, *356* (6333), 54–59.
- (4) Bhattacharjee, A.; Schnorr, K.; Oesterling, S.; Yang, Z.; Xue, T.; de Vivie-Riedle, R.; Leone, S. R. Photoinduced Heterocyclic Ring Opening of Furfural: Distinct Open-Chain Product Identification by Ultrafast X-Ray Transient Absorption Spectroscopy. *J. Am. Chem. Soc.* **2018**, *140* (39), 12538–12544. <https://doi.org/10.1021/jacs.8b07155>.

- (5) Yang, Z.; Schnorr, K.; Bhattacharjee, A.; Lefebvre, P.-L.; Epshtein, M.; Xue, T.; Stanton, J. F.; Leone, S. R. Electron-Withdrawing Effects in the Photodissociation of CH₂ICI To Form CH₂CI Radical, Simultaneously Viewed Through the Carbon K and Chlorine L_{2,3} X-Ray Edges. *J. Am. Chem. Soc.* **2018**, *140* (41), 13360–13366.
- (6) Scutelnic, V.; Tsuru, S.; Pápai, M.; Yang, Z.; Epshtein, M.; Xue, T.; Haugen, E.; Kobayashi, Y.; Krylov, A. I.; Møller, K. B.; Coriani, S.; Leone, S. R. X-Ray Transient Absorption Reveals the 1A_u (nπ*) State of Pyrazine in Electronic Relaxation. *Nat. Commun.* **2021**, *12* (1), 5003. <https://doi.org/10.1038/s41467-021-25045-0>.
- (7) Ross, A. D.; Hait, D.; Scutelnic, V.; Haugen, E. A.; Ridente, E.; Balkew, M. B.; Neumark, D. M.; Head-Gordon, M.; Leone, S. R. Jahn-Teller Distortion and Dissociation of CCl₄⁺ by Transient X-Ray Spectroscopy Simultaneously at the Carbon K- and Chlorine L-Edge. *Chem. Sci.* **2022**, *13* (32), 9310–9320. <https://doi.org/10.1039/D2SC02402K>.
- (8) Haugen, E. A.; Hait, D.; Scutelnic, V.; Xue, T.; Head-Gordon, M.; Leone, S. R. Influence of Electron Withdrawing Groups on Ultrafast Intersystem Crossing by Transient X-Ray Absorption Spectroscopy at the Carbon K-Edge. arXiv September 27, 2022. <https://doi.org/10.48550/arXiv.2209.13149>.
- (9) Epshtein, M.; Scutelnic, V.; Yang, Z.; Xue, T.; Vidal, M. L.; Krylov, A. I.; Coriani, S.; Leone, S. R. Table-Top X-Ray Spectroscopy of Benzene Radical Cation. *J. Phys. Chem. A* **2020**.
- (10) Vidal, M. L.; Epshtein, M.; Scutelnic, V.; Yang, Z.; Xue, T.; Leone, S. R.; Krylov, A. I.; Coriani, S. Interplay of Open-Shell Spin-Coupling and Jahn-Teller Distortion in Benzene Radical Cation Probed by X-Ray Spectroscopy. *J. Phys. Chem. A* **2020**.
- (11) Palmer, M. H.; Ridley, T.; Hoffmann, S. V.; Jones, N. C.; Coreno, M.; de Simone, M.; Grazioli, C.; Zhang, T.; Biczysko, M.; Baiardi, A.; Peterson, K. Interpretation of the Photoelectron, Ultraviolet, and Vacuum Ultraviolet Photoabsorption Spectra of Bromobenzene by Ab Initio Configuration Interaction and DFT Computations. *J. Chem. Phys.* **2015**, *143* (16), 164303. <https://doi.org/10.1063/1.4933419>.
- (12) Schneider, M.; Soshnikov, D. Y.; Holland, D. M. P.; Powis, I.; Antonsson, E.; Patanen, M.; Nicolas, C.; Miron, C.; Wormit, M.; Dreuw, A. A Fresh Look at the Photoelectron Spectrum of Bromobenzene: A Third-Order Non-Dyson Electron Propagator Study. *J. Chem. Phys.* **2015**, *143* (14), 144103.
- (13) Baltzer, P.; Karlsson, L.; Wannberg, B.; Öhrwall, G.; Holland, D. M. P.; MacDonald, M. A.; Hayes, M. A.; Von Niessen, W. An Experimental and Theoretical Study of the Valence Shell Photoelectron Spectrum of the Benzene Molecule. *Chem. Phys.* **1997**, *224* (1), 95–119.
- (14) Powis, I.; Holland, D. M. P.; Antonsson, E.; Patanen, M.; Nicolas, C.; Miron, C.; Schneider, M.; Soshnikov, D. Y.; Dreuw, A.; Trofimov, A. B. The Influence of the Bromine Atom Cooper Minimum on the Photoelectron Angular Distributions and Branching Ratios of the Four Outermost Bands of Bromobenzene. *J. Chem. Phys.* **2015**, *143* (14), 144304.
- (15) Hitchcock, A. P.; Pockock, M.; Brion, C. E.; Banna, M. S.; Frost, D. C.; McDowell, C. A.; Wallbank, B. Inner Shell Excitation and Ionization of the Monohalobenzenes. *J. Electron Spectrosc. Relat. Phenom.* **1978**, *13* (3), 345–360.
- (16) Hitchcock, A. P.; Fischer, P.; Gedanken, A.; Robin, M. B. Antibonding. Sigma.* Valence MOs in the Inner-Shell and Outer-Shell Spectra of the Fluorobenzenes. *J. Phys. Chem.* **1987**, *91* (3), 531–540.
- (17) Schwarz, W. H. E.; Chang, T. C.; Seeger, U.; Hwang, K. H. Core Excitations of Symmetrical Aromatic Molecules. Specific Correlations in the Valence Shell and Localization in the Core Shells. *Chem. Phys.* **1987**, *117* (1), 73–89.
- (18) Plashkevych, O.; Yang, L.; Vahtras, O.; Ågren, H.; Petterson, L. G. Substituted Benzenes as Building Blocks in Near-Edge X-Ray Absorption Spectra. *Chem. Phys.* **1997**, *222* (2–3), 125–137.
- (19) Roemelt, M.; Maganas, D.; DeBeer, S.; Neese, F. A Combined DFT and Restricted Open-Shell Configuration Interaction Method Including Spin-Orbit Coupling: Application to Transition Metal L-Edge X-Ray Absorption Spectroscopy. *J. Chem. Phys.* **2013**, *138* (20), 204101. <https://doi.org/10.1063/1.4804607>.
- (20) Becke, A. D. Density-functional Thermochemistry. III. The Role of Exact Exchange. *J. Chem. Phys.* **1993**, *98* (7), 5648–5652. <https://doi.org/10.1063/1.464913>.
- (21) Schäfer, A.; Horn, H.; Ahlrichs, R. Fully Optimized Contracted Gaussian Basis Sets for Atoms Li to Kr. *J. Chem. Phys.* **1992**, *97* (4), 2571–2577. <https://doi.org/10.1063/1.463096>.
- (22) H. Coutinho, L.; Ribeiro, F. de A.; C. Tenorio, B. N.; Coriani, S.; Santos, A. C. F. dos; Nicolas, C.; R. Milosavljevic, A.; D. Bozek, J.; Wolff, W. NEXAFS and MS-AES Spectroscopy of the C 1s and Cl 2p Excitation and Ionization of Chlorobenzene: Production of Dicationic Species. *Phys. Chem. Chem. Phys.* **2021**, *23* (48), 27484–27497. <https://doi.org/10.1039/D1CP03121J>.
- (23) Benitez, A.; Moore, J. H.; Tossell, J. A. The Correlation between Electron Transmission and Inner Shell Electron Excitation Spectra. *J. Chem. Phys.* **1988**, *88* (11), 6691–6698.
- (24) Püttner, R.; Kolczewski, C.; Martins, M.; Schlachter, A. S.; Snell, G.; Sant'Anna, M.; Viehhaus, J.; Hermann, K.; Kaindl, G. The C 1s NEXAFS Spectrum of Benzene below Threshold: Rydberg or Valence Character of the Unoccupied σ-Type Orbitals. *Chem. Phys. Lett.* **2004**, *393* (4–6), 361–366.
- (25) Kolczewski, C.; Püttner, R.; Martins, M.; Schlachter, A. S.; Snell, G.; Sant'Anna, M. M.; Hermann, K.; Kaindl, G. Spectroscopic Analysis of Small Organic Molecules: A Comprehensive Near-Edge X-Ray-Absorption Fine-Structure Study of C₆-Ring-Containing Molecules. *J. Chem. Phys.* **2006**, *124* (3), 034302.
- (26) Holland, D. M. P.; Edvardsson, D.; Karlsson, L.; Maripuu, R.; Siegbahn, K.; Potts, A. W.; von Niessen, W. An Experimental and Theoretical Study of the Valence Shell Photoelectron Spectrum of Bromobenzene. *Chem. Phys.* **2000**, *252* (1), 257–278. [https://doi.org/10.1016/S0301-0104\(99\)00346-8](https://doi.org/10.1016/S0301-0104(99)00346-8).
- (27) Krylov, A. I. Triradicals. *J. Phys. Chem. A* **2005**, *109* (47), 10638–10645.

- (28) Hait, D.; Haugen, E. A.; Yang, Z.; Oosterbaan, K. J.; Leone, S. R.; Head-Gordon, M. Accurate Prediction of Core-Level Spectra of Radicals at Density Functional Theory Cost via Square Gradient Minimization and Recoupling of Mixed Configurations. *J. Chem. Phys.* **2020**, *153* (13), 134108.
- (29) Lindblad, R.; Kjellsson, L.; Couto, R. C.; Timm, M.; Bülow, C.; Zamudio-Bayer, V.; Lundberg, M.; von Issendorff, B.; Lau, J. T.; Sorensen, S. L. X-Ray Absorption Spectrum of the N₂⁺ Molecular Ion. *Phys. Rev. Lett.* **2020**, *124* (20), 203001.
- (30) Couto, R. C.; Kjellsson, L.; Ågren, H.; Carravetta, V.; Sorensen, S. L.; Kubin, M.; Bülow, C.; Timm, M.; Zamudio-Bayer, V.; von Issendorff, B. The Carbon and Oxygen K-Edge NEXAFS Spectra of CO⁺. *Phys. Chem. Chem. Phys.* **2020**, *22* (28), 16215–16223.
- (31) Kwon, C. H.; Kim, H. L.; Kim, M. S. Vibrational Spectra of Halobenzene Cations in the Ground and \tilde{B}^2B_2 Electronic States Obtained by One-Photon Mass-Analyzed Threshold Ionization Spectrometry. *J. Chem. Phys.* **2002**, *116* (23), 10361–10371. <https://doi.org/10.1063/1.1478695>
- (32) Fally, S.; Carleer, M.; Vandaele, A. C. UV Fourier Transform Absorption Cross Sections of Benzene, Toluene, Meta-, Ortho-, and Para-Xylene. *J. Quant. Spectrosc. Radiat. Transf.* **2009**, *110* (9–10), 766–782.
- (33) Etzkorn, T.; Klotz, B.; Sørensen, S.; Patroescu, I. V.; Barnes, I.; Becker, K. H.; Platt, U. Gas-Phase Absorption Cross Sections of 24 Monocyclic Aromatic Hydrocarbons in the UV and IR Spectral Ranges. *Atmos. Environ.* **1999**, *33* (4), 525–540.
- (34) Kadi, M.; Davidsson, J.; Tarnovsky, A. N.; Rasmusson, M.; Åkesson, E. Photodissociation of Aryl Halides in the Gas Phase Studied with Femtosecond Pump-Probe Spectroscopy. *Chem. Phys. Lett.* **2001**, *350* (1), 93–98. [https://doi.org/10.1016/S0009-2614\(01\)01283-0](https://doi.org/10.1016/S0009-2614(01)01283-0).

TOC

